Wet-Chemical Synthesis of $InTaO_4$ for Photocatalytic Decomposition of Organic Contaminants in Air and Water with UV–vis Light

ARTICLE *in* INDUSTRIAL & ENGINEERING CHEMISTRY RESEARCH · JUNE 2011

Impact Factor: 2.59 · DOI: 10.1021/ie200544z

5 AUTHORS, INCLUDING:

Ruh Ullah
Curtin University
18 PUBLICATIONS **723** CITATIONS
SEE PROFILE

Shaobin Wang
Curtin University
270 PUBLICATIONS **9,285** CITATIONS
SEE PROFILE

Ha Ming Ang
Curtin University
102 PUBLICATIONS **1,954** CITATIONS
SEE PROFILE

Moses O. Tadé
Curtin University
347 PUBLICATIONS **4,157** CITATIONS
SEE PROFILE

I&EC research
Industrial & Engineering Chemistry Research

ARTICLE

pubs.acs.org/IECR

Wet-Chemical Synthesis of $InTaO_4$ for Photocatalytic Decomposition of Organic Contaminants in Air and Water with UV−vis Light

Ruh Ullah, Hongqi Sun, Shaobin Wang,* Hua Ming Ang, and Moses O. Tadé

Department of Chemical Engineering and Cooperative Research Centre for Contamination Assessment and Remediation of the Environment (CRC-CARE), Curtin University, GPO Box U1987, WA 6845, Australia

ABSTRACT: A wet-chemical technique was used to synthesize $InTaO_4$, $AgNbO_3$, $InNbO_4$, and various metal doped $InTaO_4$ catalysts. Their physicochemical properties were characterized by UV−vis diffusion reflectance spectroscopy, X-ray diffraction (XRD), scanning electron microscopy (SEM), and energy-dispersive X-ray spectroscopy (EDS). Photocatalytic activities of these materials were evaluated in liquid-phase decomposition of methylene blue and phenol as well as gas-phase degradation of toluene under UV−vis light. $InTaO_4$ exhibited higher activity than $AgNbO_3$ and $InNbO_4$ in photodecomposition of organic compounds in gas and liquid phases. Ni-doping could enhance the photocatalytic activities. Commercial TiO_2−P25 had better activity, but Ni−$InTaO_4$ showed more stable performance in catalytic oxidation of toluene.

1. INTRODUCTION

Recent investigations show that $InTaO_4$ is a good photocatalyst for splitting water to H_2 under UV light irradiation, and has better performance than commercial TiO_2−P25.[1,2] Visible light photocatalysis for water splitting and/or organic contaminant decomposition using various tantalates and niobates have also been reported.[3−5] However, $InTaO_4$ and $InNbO_4$ only showed good performance in H_2 production via visible light irradiation but less activity in O_2 production. Three important factors, (i) position of conduction/valence bands, (ii) moment of photogenerated carriers, and (iii) M−O−M angle, influence the photocatalytic activities of the materials. The more negative or positive the conduction/valence band is, the higher the redox potential is and consequently the higher photocatalytic activity presents. The more closure M−O−M is to 180°, the higher the carrier mobility is and consequently the better the activity of the material is. Zou et al.[1] demonstrated that $InTaO_4$ and $InNbO_4$ are consisted of two octahedrons, InO_6 and TaO_6/NbO_6, where conduction bands are made of empty 5d and 4d orbitals of Ta and Nb, respectively, and are positioned at different energy levels. However, valence bands which are made of O_{2p} orbitals of InO_6 in both the materials have the same potential level. Thus due to the lower conduction band position, $InNbO_4$ band gap (2.5 eV) was smaller than that of $InTaO_4$ (2.6 eV), but hydrogen was evolved at lower rate on $InNbO_4$ than that evolved on $InTaO_4$ when irradiated with visible light in the presence of cocatalyst NiO. Higher photocatalytic activity of $InTaO_4$ than $InNbO_4$ was mainly attributed to the position of the conduction band, M−O−M angle value, and its subsequent effect on electron moment. It was found that Ta−O−Ta is more closure to 180°, which alleviates moment of electron in conduction band and thus resulting in increased photocatalytic activity.

Many attempts such as doping with cations (Mn, Fe, Co, Cu, and Ni,[6] Sc, V, Zn, Ti, and Cr,[7] and anions (N)[8,9]) have been made to enhance the photocatalytic efficiency of $InTaO_4$. A significant improvement in photocatalytic production of H_2/O_2 was achieved on 1% nickel-coated $InTaO_4$, which was attributed to the alleviated electron moment caused by the change in M−O−M angle,[10] a narrowed band gap by doping,[2] and electron trapping of the NiO layer.[7]

Previously, all the above materials were prepared by solid state reaction. Some other techniques were also employed for synthesis of $InTaO_4$, such as a reactive pulsed LASER ablation method[8] and sol−gel techniques.[11] However, few investigations have been reported in wet-chemical synthesis of $InTaO_4$ or $AgNbO_3$, which is usually facile and environmentally friendly, and their application for decomposition of organic contaminants.[9] Hiroshi et al.[9] found that $InTaO_4$ doped with vanadium could decompose gaseous isopropyl alcohol (IPA) into acetone and CO_2 at ultraviolet radiation but showed little activity under visible light irradiation. Chiou et al.[11] reported that $InTaO_4$ prepared by sol−gel techniques demonstrated higher photocatalytic activities for H_2 production because of a smaller band gap (2.62 eV), particle size (0.05−0.1 μm), and more uniform crystalline phase compared to the one prepared by solid state reactions.

Photocatalytic decomposition of contaminants in gas and water is important in environmental remediation.[12−14] Many types of photocatalyst have been tested; however, few investigations have been reported using $InTaO_4$ systems. In this paper, we report synthesis of pristine $InTaO_4$, $AgNbO_3$, $InNbO_4$, and doped $InTaO_4$ by a simple wet-chemical technique. The synthesized materials were tested for photocatalytic decomposition of methylene blue in aqueous solution and toluene in gaseous phase under UV−vis light.

2. EXPERIMENTAL SECTION

2.1. Synthesis of Various Catalysts. Polycrystalline pristine $InTaO_4$, $AgNbO_3$, $InNbO_4$, and doped $InTaO_4$ photocatalysts

Special Issue: Nigam Issue

Received: March 18, 2011
Accepted: June 21, 2011
Revised: June 20, 2011
Published: June 21, 2011

dx.doi.org/10.1021/ie200544z | *Ind. Eng. Chem. Res.* 2012, 51, 1563–1569

were prepared by a solution method. All of chemicals were obtained from Sigma-Aldrich at 99.99% purity and were used as received. In a typical synthesis, 10 mmol of indium(III) nitrate hydrate ($In(NO_3)_3 \cdot xH_2O$) and 8 mmol of tantalum(V) chloride ($TaCl_5$) were dissolved separately in a 50-mL ethanol solution with continuously stirring and heating at 70 °C for 30 min to make solutions A and B, respectively. Dopant solution C was also prepared similarly by dissolving 0.01 mmol of dopant salt (cobalt(II) nitrate hexahydrate, copper(II) nitrate trihydrate, and nickel(II) nitrate hexahydrate, etc.) in 30 mL of ethanol. Both solutions A and B were then mixed and 0.5−1.0 mL of concentrated nitric acid was added to the mixture. The mixture was kept heating at 80 °C for refluxing of 6−8 h. A clear solution without any precipitation was then aged for 12−24 h at room temperature and then kept in an oven at 50−60 °C until dried completely. After being ground, the samples were calcined at 1150 °C for 24−30 h. $AgNbO_3$ and $InNbO_4$ were also prepared by the similar technique where niobium(V) chloride ($NbCl_5$) and silver nitrate ($AgNO_3$) were used as Nb and Ag precursors, respectively.

2.2. Characterization of Catalysts. The crystal structures of samples were analyzed by X-ray diffractometer (Bruker D8 Advance equipped with a Lynx eye detector, Bruker-AXS, Karlsruhe, Germany) operated at 40 kV and 30 mA. The scanning rate was 0.2 s/step with 2θ (10°−90°) and step size of 0.02°. Cu Kα (λ = 1.54178 Å) was used as a X-ray source with divergent slit of 0.300 and 2.5° primary and secondary soller slits. The optical absorption of samples was determined by UV−vis absorbance spectroscopy using the diffuse reflectance method (JASCO V-670 Spectrometer). Morphology and chemical compositions of the materials were examined by scanning electron microscopy (ZEISS NEON 40EsB) equipped with an energy dispersive spectrometer (SEM-EDS). Surface chemistry of catalyst samples was examined by X-ray photoelectron spectroscopy (XPS) and FTIR analyses. FTIR analysis was performed on a Perkin-Elmer model FTIR-100 with a MIR detector. XPS data were acquired using a Kratos Axis ULTRA X-ray photoelectron spectrometer incorporating a 165-mm hemispherical electron energy analyzer. The incident radiation was monochromatic Al Kα X-rays (1486.6 eV) at 225 W (15 kV, 15 mA). Survey (wide) scans were taken at analyzer pass energy of 160 eV and multiplex (narrow) high-resolution scans at 40 eV. Survey scans were carried out over 1200.0 eV binding energy range with 1.0 eV steps and a dwell time of 100 ms. Narrow high-resolution scans were run with 0.05 eV steps and 250 ms dwell time.

2.3. Photocatalytic Evaluation. Photocatalytic activities of prepared samples were evaluated in decomposition of methylene blue in water and toluene in air with UV−vis radiations. The light source was a 500 W mercury−xenon lamp (UXM-502MD, Ushio) with average intensities of 5 mW/cm^2 at 220−280 nm, 38.5 mW/cm^2 at 280−400 nm, and 200 mW/cm^2 at >400 nm. In a typical run of methylene blue decomposition in water, 10 ppm methylene blue solution with 100 mg of catalyst particles were continuously stirred in a Pyrex glass reactor which was irradiated with the UV−vis light without any filter. Temperature of the reactor was maintained by passing cooling water through the reactor continuously. Concentration of methylene blue was determined by taking 1-mL aliquots from the reactor at regular intervals. The aliquots were evaluated by measuring the absorbance at λ = 664 nm on a visible spectrophotometer (Spectronic Instruments model 4001/4).

Toluene decomposition in gas was evaluated in a flow reactor connected with a gas chromatograph (Shimadzu GC-17A) fitted with a GS-GSPRO column of 60 m long and 0.32 mm inner diameter. Oven temperature of the GC was 220 °C and FID detector temperature was kept at 250 °C. In a typical experiment, 200−300 mg of a photocatalyst was dispersed in 10 mL of deionized water in a Petri dish of 450-mm diameter and was dried in an oven overnight. The Petri dish was kept inside an airtight reactor fitted with a removable quartz sheet in order to allow UV−vis radiation in. A flow of toluene at 100 ppm was continuously passed into the reactor (1.08 L) at a flow rate of 60 mL/min. The temperature of the reactor was controlled at room temperature by continuously passing cooling water through the reactor and also by blowing the reactor with fresh air from outside.

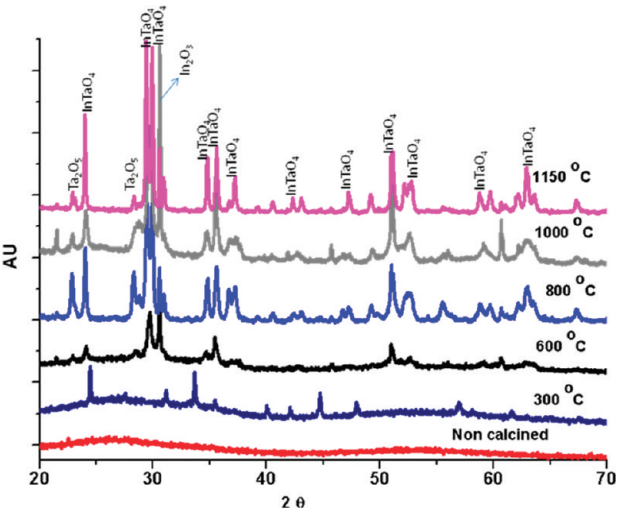

Figure 1. XRD analysis of $InTaO_4$ synthesized at various temperatures.

3. RESULTS AND DISCUSSION

3.1. Characterization of Catalysts. XRD analysis of the prepared $InTaO_4$ calcined at varying temperatures (Figure 1) indicates that the sample without calcination presented an amorphous phase. However, crystallization could be observed at calcination of 300 °C and complete crystalline structure of $InTaO_4$ was obtained at elevated temperature of 1150 °C. At lower temperatures (300−1000 °C), In_2O_3 and Ta_2O_5 at 2θ = 30.58°, 21.47° and 2θ = 22.820°, 28.267°, respectively, were observed. However, indium tantalum oxide ($InTaO_4$) was found to be the major product, which has a monoclinic structure with a = 5.150, b = 5.770, c = 4.821, α = 90.0°, β = 91.35°, γ = 90.0°, primitive $P2/a$ (13). This $InTaO_4$ has a crystal structure similar to those prepared by solid state reaction, but in different space group of $P2/c$.[1]

To obtain a pure product of $InTaO_4$, molar ratios of the precursor salts (indium nitrate and tantalum chloride) were varied in preparation. It was found that the sample synthesized at the molar ratio of 1:0.5 (In:Ta) had much lower In_2O_3 and Ta_3O_5 impurities (Figure 2). Therefore, the molar ratio of In:Ta was kept at 1:0.5 for doped $InTaO_4$ synthesis. The metals of doping were Bi, Cu, Ag, V, and Ni at 1−2%. XRD patterns (Figure 3) showed no significant structure change occurring on those doped samples. This revealed that 1−2% metal doping into pristine $InTaO_4$ may only bring about some physical changes but no changes in crystalline structure or chemical phase.[2] Zou et al.[10] also reported no modification in crystalline parameters

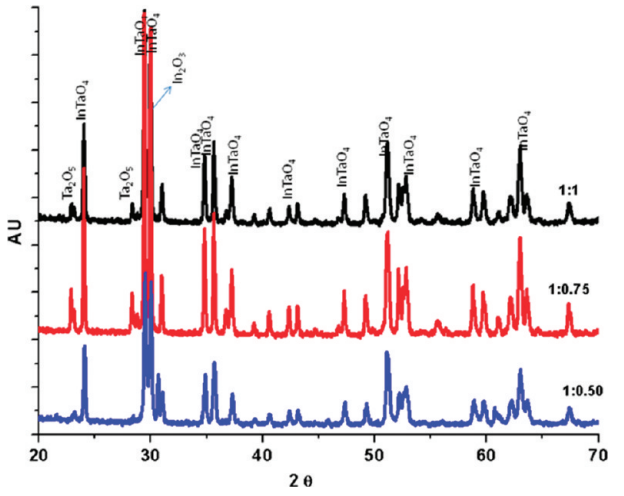

Figure 2. XRD analysis of $InTaO_4$ synthesized at different ratios of In and Ta.

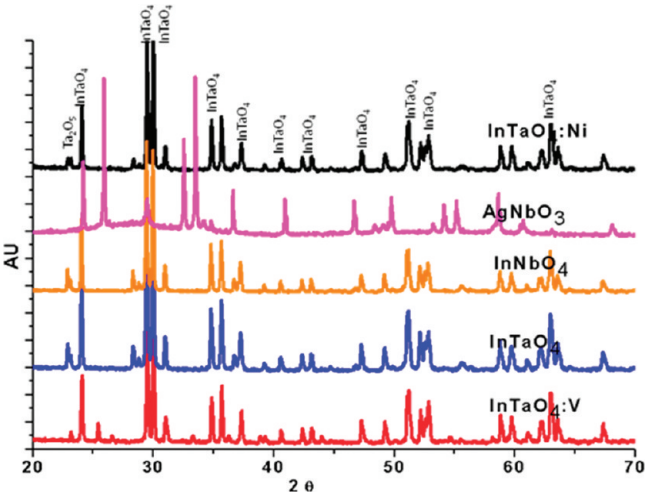

Figure 3. XRD analysis of $AgNbO_3$, $InNbO_4$, and Ni-, V-doped $InTaO_4$ catalysts.

by doping $InTaO_4$ with Ag, Ni, Cu, and Co. However, a slight decrease in crystal parameters (a = 4.833, b = 5.778, c = 5.157, α = 90.000°, β = 91.380°, γ = 90.000°) was found in bismuth doped sample ($InTaO_4$:Bi). The steadiness of crystal structure and crystal parameters of $InTaO_4$ by doping with Ag^{2+}, Ni^{2+}, Cu^{2+}, and Co^{2+} may be due to either their interstitial position or surface cover of the oxides on $InTaO_4$. Bismuth with different ionic radius may cause the structural variation. Thus it is concluded that substitutional dopant could cause variations in crystal parameters if the dopant ionic size is different from that of the substituted ion while the interstitial doping of foreign elements may only change the physical properties such as an increase in defect sites and band gap modification.

XRD analyses of $AgNbO_3$ and $InNbO_4$ (Figure 3) show that silver niobium oxide ($AgNbO_3$) has an orthorhombic structure with a = 5.602, b = 7.824, c = 5.540, α = 90.000, β = 90.000, γ = 90.0, primitive *Pnma* (62). Indium niobium oxide has a monoclinic structure with a = 4.843, b = 5.773, c = 5.147, α = 90.0°, β = 91.230°, and γ = 90.0°, Primitive $P2/c$. Chemical compositions of doped and nondoped samples determined by SEM-EDS

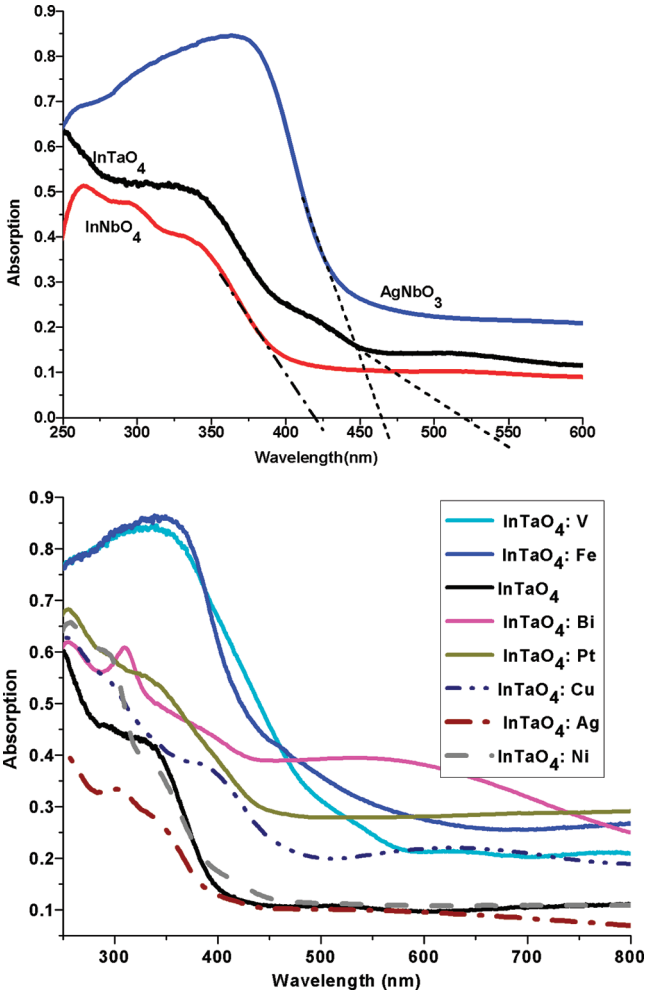

Figure 4. UV−vis diffusive reflectance spectra of $AgNbO_3$, $InNbO_4$, $InTaO_4$, and metal-doped $InTaO_4$.

show no dopant atoms, which is probably due to the low contents of dopants.

UV−vis diffuse reflectance spectra of nondoped and doped $InTaO_4$ (Figure 4) indicate that doping of metal ions to $InTaO_4$ brought out a significant change to the absorption profile by extending strong absorption to visible range. Figure 4 shows that there is a shoulder peak between 284 and 340 nm in the optical absorption of pristine $InTaO_4$, which reveals that this material may have two band gaps. The absorption edge at around 284 nm is due to the electronic transition between conduction band and valence band, and another absorption edge at around 450 nm is because of the defect sites mostly being composed of oxygen vacancies. Hiroshi et al.[9] have also observed the similar effect of two onsets in the absorption spectrum of nondoped $InTaO_4$. The band gap of the nondoped $InTaO_4$ estimated with a formula[15] (Eg = 1239/λ (wavelength nm)) was found to be 2.4 eV,[16] however, Zou et al.[10] reported a band gap of 2.6 eV for a nondoped $InTaO_4$. Although there are different views[17] regarding the band gap due to the two onsets in the absorption spectrum of $InTaO_4$, however, based on its first absorption edge at lower wavelength, this material has a larger and indirect band gap of 4.3 eV.[8,9]

Figure 4 also shows the optical absorption of $AgNbO_3$ and $InNbO_4$. $InTaO_4$ and $AgNbO_3$ have an onset at 400 and 450 nm,

dx.doi.org/10.1021/ie200544z |*Ind. Eng. Chem. Res.* 2012, 51, 1563–1569

Scheme 1. Band Gap Modification of $InTaO_4$ Doped with Various Ions (Bi, Cu, Ni)

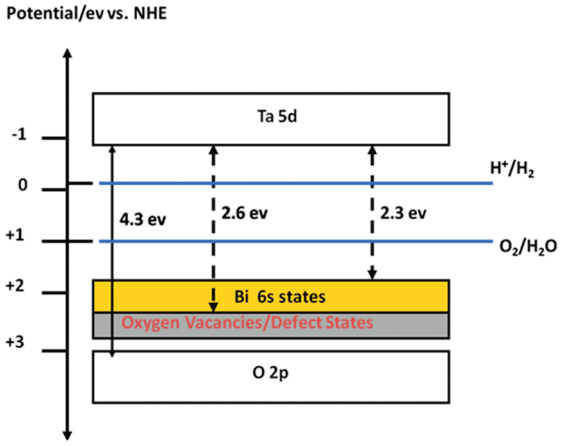

respectively, while $InNbO_4$ has an absorption onset at lower wavelength of 380 nm. Unlike $InTaO_4$, $AgNbO_3$ has very sharp absorption, whereas $InNbO_4$ has a flat shoulder absorption between 280 and 380 nm. Band gaps of $InNbO_4$ and $AgNbO_3$ were found to be 2.9 eV and 2.8 eV, respectively. Ye et al.[18] reported a band gap of 2.5 eV for $InNbO_4$ and Li et al.[19] reported a similar band gap of 2.8 eV for $AgNbO_3$.

Doping Pt, Cu, Ag, Ni, Co, Fe, and Bi ions in $InTaO_4$ modified the optical absorption of $InTaO_4$ and shifted the absorption to the longer wavelength (Figure 4). This red-shift in doped $InTaO_4$ was also reported by other investigators.[7,9] Dopants like Fe, V, Bi, and Cu enhanced the optical absorption significantly and produced a shift of absorption edge to the longer wavelength, whereas Ag doping had a worse effect on the optical absorption by reducing the overall optical absorption. Dopant ions like Bi, Fe, V, and Cu would substitute In ions in InO_6 octahedron and brought out changes to the crystal structure in lattice parameters reducing the band gap. The changes in lattice parameters also affected the volume of InO_6 octahedron producing defect sites and enhancing optical absorption.

As illustrated in Scheme 1, dopants like Bi, Fe, V, and Cu introduced a narrow band just above the valence band of $InTaO_4$, and pushed the valence band toward more negative position, thus reducing the effective band gap of $InTaO_4$. Therefore, owing to the above two reasons, i.e., increase in defect sites, and formation of dopant band above the valence band, doped $InTaO_4$ absorbed more light in the visible range. Contrary to Bi, Fe, V, and Cu ions doping, Ni doping into $InTaO_4$ brought about very limited modification to the optical absorption while it induced a moderate increase in UV light absorption (Figure 4). This effect of different absorption characteristics at longer or shorter wavelengths suggests that different dopant ions may have different positions (interstitial, substitution) in the crystal thus producing defect states at various energy levels. We suggest that Ni ion doping induces both deep and shallow defect states, which promote the absorption mostly in shorter wavelength and minor changes at longer wavelengths. It must be noted that various reports[1,2] on Ni-doped $InTaO_4$ have suggested internal transitions in partially filled Ni 3d levels, which boosted absorption both in the longer and shorter wavelengths. However, XPS analysis (discussion later) confirmed the presence of Ni^{2+} 2p state, which meant that NiO is formed on the surface of $InTaO_4$.

Scheme 2. Diagram of Ni-doped $InTaO_4$ in Photocatalysis

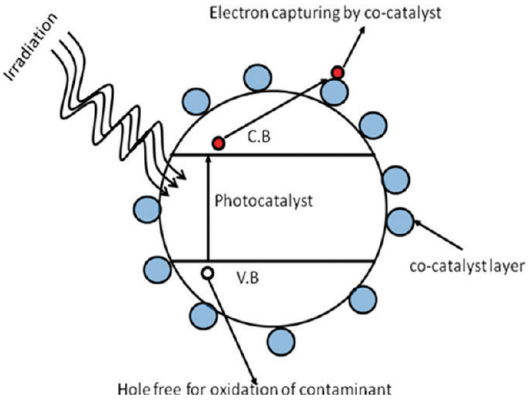

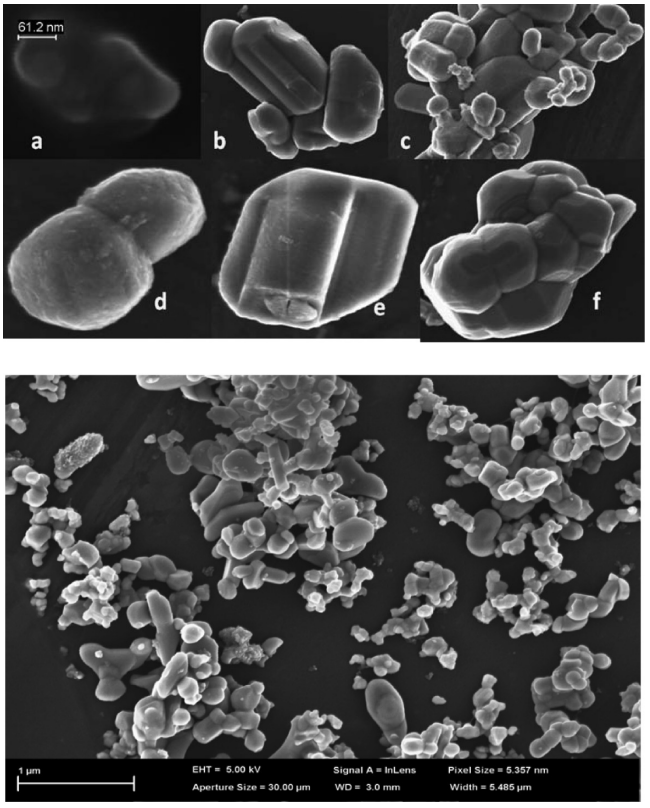

Figure 5. SEM images of $InTaO_4$ (a−d) and Ni-doped $InTaO_4$ (e−g).

The presence of NiO on the surface acts as cocatalyst and traps the photogenerated electrons, thus reducing the electron−hole pair recombination. This electron trapping (Scheme 2) of the cocatalyst (NiO) can not produce a significant modification to the band gap but assist in suppression of electron−hole recombination process.

SEM images (Figure 5a−d) of nondoped $InTaO_4$ show the presence of varying geometrical shapes and particle sizes, i.e., elongated, spherical, and plate-like structures. These images suggested the growth and agglomeration of $InTaO_4$. SEM images of Ni doped $InTaO_4$ (Figure 5e−g) show similar particles morphology and particle size as that of nondoped $InTaO_4$, suggesting that doping did not change the morphology of $InTaO_4$. SEM image (Figure 6) of $InNbO_4$ shows that this

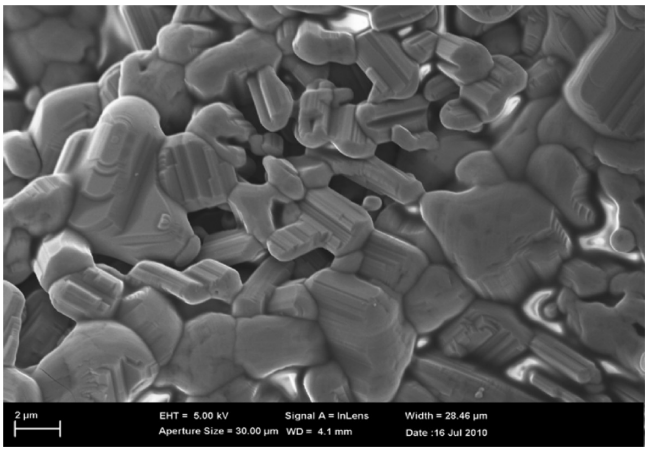

Figure 6. SEM image of $InNbO_4$.

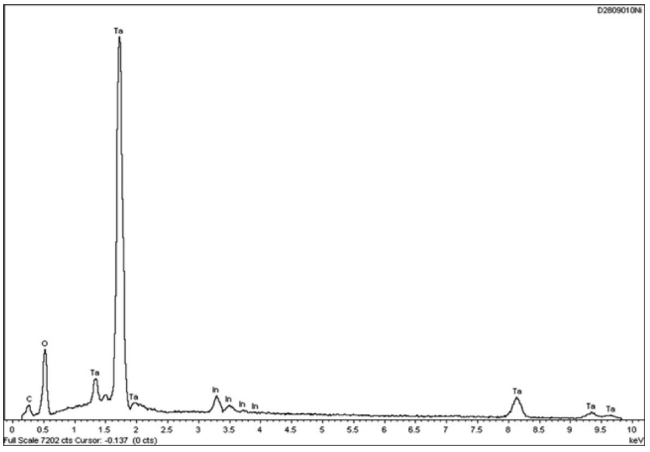

Figure 7. EDS analysis of $InTaO_4$:Ni.

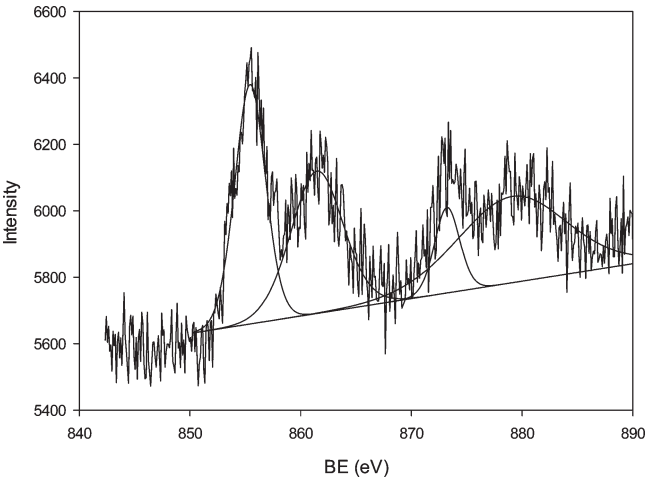

Figure 8. XPS Ni 2p spectrum of $InTaO_4$:Ni.

material crystallizes in plate-like structure and has a comparatively larger microsize to that of $InTaO_4$.

Although EDS (Figure 7) and XRD investigations could not detect Ni and/or NiO, however, XPS of Ni doped $InTaO_4$ confirmed the existence of NiO (Figure 8). Ni $2p_{3/2}$ state of NiO

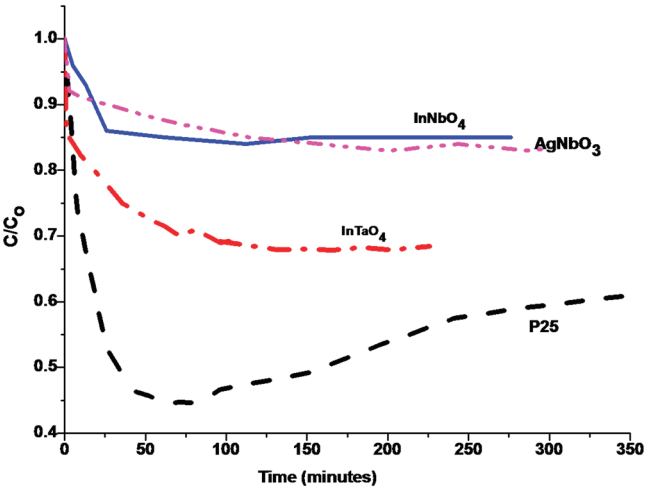

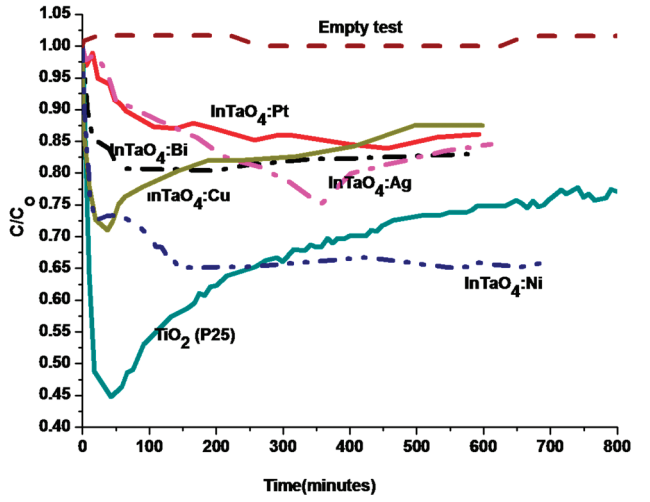

Figure 9. Photocatalytic decomposition of toluene on various photocatalysts with UV−vis irradiation.

was observed at binding energy (BE) of 855.5 eV[11] where its corresponding satellite peak is close to 861.0 eV. The satellite is about 6.0 eV higher than the main BE peak. Another peak observed at 873.6 eV can be assigned to Ni $2p_{1/2}$ states of NiO.[20] Chiou et al.[11] also observed the presence of metallic Ni at binding energy of 852.9 eV, of the sample reduced in H_2 environment. However, we could not observe existence of metallic Ni[21] in the Ni-doped sample of $InTaO_4$.

Therefore, XRD and SEM-EDS analyses show that doping at 1−2% in $InTaO_4$ would not change its bulk and structural composition, but doping could modify the photoresponsive properties of $InTaO_4$ inducing a change in photocatalytic behavior.

3.2. Photocatalytic Activities. Photocatalytic activities of $InTaO_4$, $InNbO_4$, $AgNbO_3$, and doped $InTaO_4$ catalysts in decomposition of toluene gas were determined in a closed continuous-flow reactor irradiated with UV−vis light (Figure 9). TiO_2−P25 presented a fast decomposition of toluene at 50% in the first hour under UV−vis irradiation but strong deactivation afterward. After 800 min, toluene decomposition efficiency was reduced to 20%. $InTaO_4$ exhibited a gradually increased efficiency of toluene degradation and reached 30% at the first hour and maintained the stable activity after. $InNbO_4$ and $AgNbO_3$[22]

dx.doi.org/10.1021/ie200544z |*Ind. Eng. Chem. Res.* 2012, 51, 1563–1569

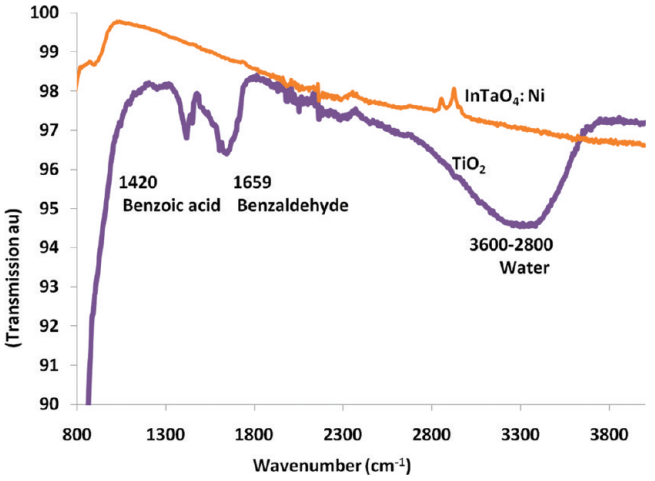

Figure 10. FTIR spectra of used TiO_2 and $InTaO_4$:Ni.

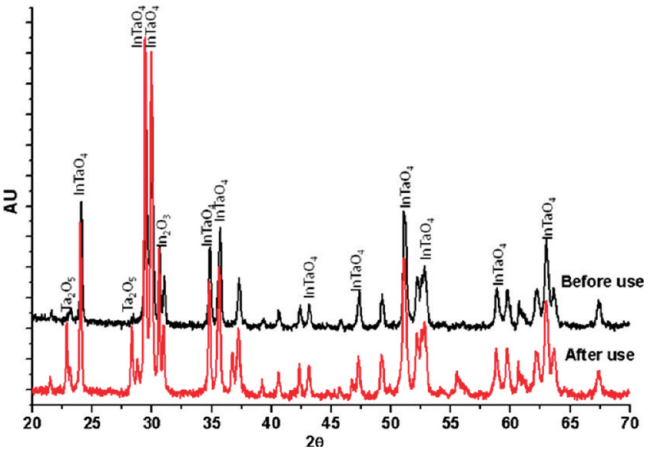

Figure 11. XRD analaysis of $InTaO_4$:Ni before and after use for photocatalytic reaction.

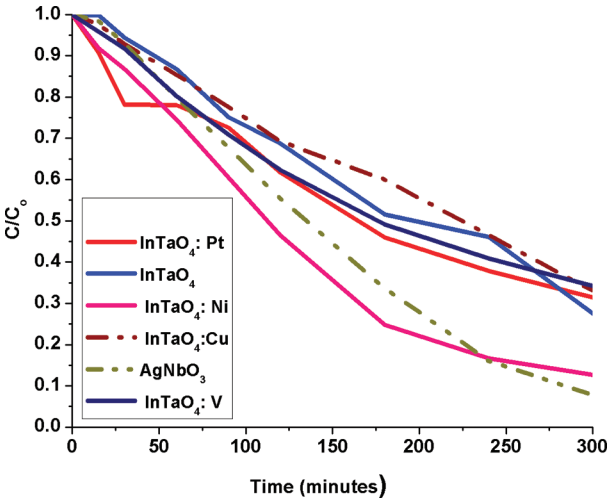

Figure 12. Decomposition of methylene blue on various photocatalysts with UV−vis irradiation.

showed similar activities with decomposition of toluene at 10−15% within the first 2 h. The deactivation of TiO_2−P25 was due to a strong affinity to water and reaction intermediates which covered the surface reactive sites for photocatalytic decomposition of toluene. It was also found that TiO_2−P25 changed the color from white to black after reaction; however $InTaO_4$ showed a pale yellow indicating much less intermediate adsorption on the surface.

Figure 10 shows FTIR analysis of TiO_2−P25 and $InTaO_4$ after use for photocatalytic oxidation of toluene under UV−vis light irradiation. Similar to other research work,[23−25] strong water and intermediate adsorption was observed on TiO_2 surface. A broad and intense peak at 2800−3600 cm^{-1} centered at 3350 cm^{-1} corresponds to the stretching mode of water molecules[23] whereas the band at 1590−1700 cm^{-1} centered at 1659 cm^{-1} corresponds to aromatic molecules of benzaldehyde. Another aromatic intermediate observed with a single band at 1420 cm^{-1} was found to be benzoic acid.[23,26] It can be deduced from the FTIR analysis that strong adsorption of water molecules and aromatic intermediates covered the active sites of TiO_2 and caused the irreversible deactivation.[26,27] However, such strong adsorption of water molecules and intermediates did not occur on doped and nondoped $InTaO_4$ surface and therefore they would work longer than the commercial TiO_2.

Photocatalytic activity of Ni, Ag, Cu, Pt, and Bi doped $InTaO_4$ samples for toluene decomposition were also investigated (Figure 9). The order of photocatalytic activity in the first 2 h was TiO_2−P25 > $InTaO_4$:Ni > $InTaO_4$:Cu > $InTaO_4$:Bi > $InTaO_4$:Ag > $InTaO_4$:Pt. As shown in Figure 9, the tests in a longer period indicated that Ni-doped $InTaO_4$ was far better than the commercial TiO_2−P25. The activity of $InTaO_4$:Ni remained unchanged in 14 h. In the second run after regeneration, TiO_2−P25 lost 90% of its efficiency, while $InTaO_4$:Ni maintained its photocatalytic activity. XRD anaylsis of $InTaO_4$:Ni after reaction for 14 h (Figure 11) clearly indicates that the material was quite stable and did not change its structure. This strong stability of the material suggests that $InTaO_4$ doped with Ni can be a better alternative to the commercial photocatalytic material TiO_2−P25. Zou et al.[22] found that TiO_2−P25 had better performance than Ni-doped $InTaO_4$ in H_2 production from water splitting under UV light irradiation. However, $InTaO_4$ doped with Mn, Co, and Ni showed better performance than TiO_2−P25 for H_2 production under visible light irradiation.[2,10] Chiou et al.[11] have demonstrated that 3 wt % Ni loading produced both NiO and NiOH on $InTaO_4$ surface. Upon reduction in H_2 environment metallic Ni shell on surface was created and acted as electron trapping centers, enhancing photocatalytic water splitting. Thus it is deduced that the better performance of $InTaO_4$:Ni is the combined effect of both the band gap contraction and electron capturing by NiO as explained in Scheme 2. Although doping of $InTaO_4$ with Ag, Cu, Pt, V, and Bi produced red-shifts of the optical absorption but they did not make a cover on the $InTaO_4$ surface like NiO. These metal dopants reduced the optical band gap, but they may also enhance the electron−hole pair recombination, by creating midgap defect states. The generation of the defect states plays a detrimental role in recombination centers which may reduce the photocatalytic decomposition of toluene. Ni doping modified the band gap but suppressed the recombination via electron trapping on NiO, making it exhibit better performance. Recently, Shu et al.[22] have demonstrated a similar effect of electron trapping by NiO loaded on $AgNbO_3$ for methylene blue decomposition under UV irradiation.

Photocatalytic performance of nondoped and doped $InTaO_4$ materials in methylene blue decomposition in water with UV−vis light (Figure 12) showed that Ni-doped $InTaO_4$ degraded methylene blue at a much faster rate than the others.

$AgNbO_3$ had performance almost comparable to $InTaO_4$:Ni. $InTaO_4$:Ni and $AgNbO_3$ were capable of decomposing about 90% methylene blue within 6 h, while Cu, Pt, V, and nondoped $InTaO_4$ could degrade about 60% methylene blue. It is noted that doped and nondoped $InTaO_4$ did not show the same trend in methylene blue decomposition as that in toluene decomposition; however, Ni-doped $InTaO_4$ has demonstrated the best performance. Another test revealed that Ni-doped $InTaO_4$ could also decompose about 75% of phenol within 3 h (figure not shown). As explained earlier, the better photocatalytic performance of Ni-doped $InTaO_4$ among the others are mainly attributed to the dual effects of band gap reduction and electron trapping by NiO.

4. CONCLUSIONS

Tantalum- and niobium-based compounds such as $InTaO_4$, $InNbO_4$, and $AgNbO_3$ can be prepared by a simple wet-chemical technique. Most of these materials possess poly crystalline structures and large size agglomerates. $InTaO_4$ exhibits better activity than $InNbO_4$ and $AgNbO_3$. The physical properties and photocatalytic activities of $InTaO_4$ are also influenced by doping with metals like Pt, Cu, Ag, V, Bi, and Ni. Bi-doped $InTaO_4$ will result in more visible light absorption, but Ni-doped $InTaO_4$ shows stronger UV absorption. $InTaO_4$:Ni can efficiently decompose all the contaminants of toluene, methylene blue, and phenol in air or water under UV−vis light. The higher photocatalytic activity of $InTaO_4$:Ni is attributed to the band gap modification and electron trapping center of NiO. $InTaO_4$:Ni also has better performance in multiple uses and longer lifetime than the commercial TiO_2−P25.

AUTHOR INFORMATION

Corresponding Author

*E-mail: Shaobin.wang@curtin.edu.au.

REFERENCES

(1) Zou, Z.; Ye, J.; Arakawa, H. Structural properties of $InNbO_4$ and $InTaO_4$: Correlation with photocatalytic and photophysical properties. *Chem. Phys. Lett.* **2000**, *332* (3−4), 271–277.

(2) Zou, Z.; Ye, J.; Sayama, K.; Arakawa, H. Photocatalytic hydrogen and oxygen formation under visible light irradiation with M-doped $InTaO_4$ (M = Mn, Fe, Co, Ni and Cu) photocatalysts. *J. Photochem. Photobiol., A* **2002**, *148* (1−3), 65–69.

(3) Yang, X.; Xu, L.; Yu, X.; Li, W.; Li, K.; Huo, M.; Guo, Y. Enhanced photocatalytic activity of Eu_2O_3/Ta_2O_5 mixed oxides on degradation of rhodamine B and 4-nitrophenol. *Colloids Surf., A* **2008**, *320* (1−3), 61–67.

(4) Ohuchi, T.; Miyatake, T.; Hitomi, Y.; Tanaka, T. Liquid phase photooxidation of alcohol over niobium oxide without solvents. *Catal. Today* **2007**, *120* (2), 233–239.

(5) Zhang, G.; Hu, Y.; Ding, X.; Zhou, J.; Xie, J. Wet chemical synthesis and photocatalytic activity of potassium niobate $K_6Nb_{10.8}O_{30}$ powders. *J. Solid State Chem.* **2008**, *181* (9), 2133–2138.

(6) Zhang, X.; Ai, Z.; Jia, F.; Zhang, L. Generalized one-pot synthesis, characterization, and photocatalytic activity of hierarchical BiOX (X = Cl, Br, I) nanoplate microspheres. *J. Phys. Chem. C* **2008**, *112* (3), 747–753.

(7) Ye, J.; Zou, Z. Visible light sensitive photocatalysts $In_{1-x}M_xTaO_4$ (M = 3d transition-metal) and their activity controlling factors. *J. Phys. Chem. Solids* **2005**, *66* (2−4), 266–273.

(8) Matsushima, S.; Obata, K.; Nakamura, H.; Arai, M.; Kobayashi, K. First-principles energy band calculation for undoped and N-doped $InTaO_4$ with layered wolframite-type structure. *J. Phys. Chem. Solids* **2003**, *64* (12), 2417–2421.

(9) Hiroshi, I.; Kazuhito, H. Visible light-sensitive $InTaO_4$-based photocatalysts for organic decomposition. *J. Am. Ceram. Soc.* **2005**, *88* (11), 3137–3142.

(10) Zou, Z.; Ye, J.; Sayama, K.; Arakawa, H. Direct splitting of water under visible light irradiation with an oxide semiconductor photocatalyst. *Nature* **2001**, *414* (6864), 625–627.

(11) Chiou, Y.-C.; Kumar, U.; Wu, J. C. S. Photocatalytic splitting of water on $NiO/InTaO_4$ catalysts prepared by an innovative sol-gel method. *Appl. Catal., A* **2009**, *357* (1), 73–78.

(12) Wang, S. B.; Ang, H. M.; Tade, M. O. Volatile organic compounds in indoor environment and photocatalytic oxidation: State of the art. *Environ. Int.* **2007**, *33* (5), 694–705.

(13) Shukla, P.; Fatimah, I.; Wang, S.; Ang, H. M.; Tadé, M. O. Photocatalytic generation of sulphate and hydroxyl radicals using zinc oxide under low-power UV to oxidise phenolic contaminants in wastewater. *Catal. Today* **2010**, *157* (1−4), 410–414.

(14) Shukla, P. R.; Wang, S.; Ang, H. M.; Tadé, M. O. Photocatalytic oxidation of phenolic compounds using zinc oxide and sulphate radicals under artificial solar light. *Sep. Purif. Technol.* **2010**, *70* (3), 338–344.

(15) Zhang, K. L.; Liu, C. M.; Huang, F. Q.; Zheng, C.; Wang, W. D. Study of the electronic structure and photocatalytic activity of the BiOCl photocatalyst. *Appl. Catal., B* **2006**, *68* (3−4), 125–129.

(16) Madhusudan Reddy, K.; Manorama, S. V.; Ramachandra Reddy, A. Bandgap studies on anatase titanium dioxide nanoparticles. *Mater. Chem. Phys.* **2003**, *78* (1), 239–245.

(17) Chang, H.; Kong, K.; Choi, Y. S.; In, E.; Choi, Y.; Baeg, J.-O.; Moon, S.-J. Electronic structures of $InTaO_4$, a promising photocatalyst. *Chem. Phys. Lett.* **2004**, *398* (4−6), 449–452.

(18) Ye, J.; Zou, Z.; Arakawa, H.; Oshikiri, M.; Shimoda, M.; Matsushita, A.; Shishido, T. Correlation of crystal and electronic structures with photophysical properties of water splitting photocatalysts $InMO_4$ ($M = V^{5+}, Nb^{5+}, Ta^{5+}$). *J. Photochem. Photobiol., A* **2002**, *148* (1−3), 79–83.

(19) Li, G.; Kako, T.; Wang, D.; Zou, Z.; Ye, J. Composition dependence of the photophysical and photocatalytic properties of $(AgNbO_3)_{1-x}(NaNbO_3)_x$ solid solutions. *J. Solid State Chem.* **2007**, *180* (10), 2845–2850.

(20) Suwanwatana, W.; Yarlagadda, S.; Gillespie, J. J. W. Hysteresis heating based induction bonding of thermoplastic composites. *Compos. Sci. Technol.* **2006**, *66* (11−12), 1713–1723.

(21) Dutta, R. S.; Jagannath; Dey, G. K.; De, P. K. Characterization of microstructure and corrosion properties of cold worked Alloy 800. *Corros. Sci.* **2006**, *48* (9), 2711–2726.

(22) Shu, H.; Xie, J.; Xu, H.; Li, H.; Gu, Z.; Sun, G.; Xu, Y. Structural characterization and photocatalytic activity of $NiO/AgNbO_3$. *J. Alloys Compd.* **2010**, *496* (1−2), 633–637.

(23) Barraud, E.; Bosc, F.; Edwards, D.; Keller, N.; Keller, V. Gas phase photocatalytic removal of toluene effluents on sulfated titania. *J. Catal.* **2005**, *235* (2), 318–326.

(24) Martra, G.; Coluccia, S.; Marchese, L.; Augugliaro, V.; Loddo, V.; Palmisano, L.; Schiavello, M. The role of H_2O in the photocatalytic oxidation of toluene in vapour phase on anatase TiO_2 catalyst: A FTIR study. *Catal. Today* **1999**, *53* (4), 695–702.

(25) Augugliaro, V.; Coluccia, S.; Loddo, V.; Marchese, L.; Martra, G.; Palmisano, L.; Schiavello, M. Photocatalytic oxidation of gaseous toluene on anatase TiO_2 catalyst: Mechanistic aspects and FT-IR investigation. *Appl. Catal., B* **1999**, *20* (1), 15–27.

(26) Marcì, G.; Addamo, M.; Augugliaro, V.; Coluccia, S.; García-López, E.; Loddo, V.; Martra, G.; Palmisano, L.; Schiavello, M. Photocatalytic oxidation of toluene on irradiated TiO_2: Comparison of degradation performance in humidified air, in water and in water containing a zwitterionic surfactant. *J. Photochem. Photobiol., A* **2003**, *160* (1−2), 105–114.

(27) Maira, A. J.; Coronado, J. M.; Augugliaro, V.; Yeung, K. L.; Conesa, J. C.; Soria, J. Fourier transform infrared study of the performance of nanostructured TiO_2 particles for the photocatalytic oxidation of gaseous toluene. *J. Catal.* **2001**, *202* (2), 413–420.